

MITRAL CELL PRESYNAPTIC  $\text{Ca}^{2+}$  INFLUX AND SYNAPTIC TRANSMISSION IN FROG AMYGDALA

S. J. MULLIGAN,\* I. DAVISON and K. R. DELANEY

Department of Biological Sciences, Simon Fraser University, Burnaby, B.C., Canada V5A 1S6

**Abstract**—Dextran-conjugated  $\text{Ca}^{2+}$  indicators were injected into the accessory olfactory bulb of frogs *in vivo* to selectively fill presynaptic terminals of mitral cells at their termination in the ipsilateral amygdala. After one to three days of uptake and transport, the forebrain hemisphere anterior to the tectum was removed and maintained *in vitro* for simultaneous electrophysiological and optical measurements.  $\text{Ca}^{2+}$  influx into these terminals was compared to synaptic transmission between mitral cells and amygdala neurons under conditions of reduced  $\text{Ca}^{2+}$  influx resulting from reduced extracellular  $[\text{Ca}^{2+}]_o$ , blockade of N- and P/Q-type channels, and application of the cholinergic agonist carbachol. Reducing extracellular  $[\text{Ca}^{2+}]_o$  had a non-linear effect on release; release was proportional to  $\text{Ca}^{2+}$  influx raised to the power of  $\approx 3.6$ , as observed at numerous other synapses. The N-type  $\text{Ca}^{2+}$  channel blocker,  $\omega$ -conotoxin-GVIA (1  $\mu\text{M}$ ), blocked 77% of  $\text{Ca}^{2+}$  influx and 88% of the postsynaptic field potential. The P/Q-type  $\text{Ca}^{2+}$  channel blocker,  $\omega$ -agatoxin-IVA (200 nM), blocked 19% of  $\text{Ca}^{2+}$  influx and 25% of the postsynaptic field, while the two toxins combined to block 92% of  $\text{Ca}^{2+}$  influx and 97% of the postsynaptic field. The relationship between toxin blockade of  $\text{Ca}^{2+}$  influx and synaptic transmission was therefore only slightly non-linear; release was proportional to  $\text{Ca}^{2+}$  influx raised to the power  $\approx 1.4$ . Carbachol (100  $\mu\text{M}$ ) acting via muscarinic receptors had no effect on the afferent volley, but rapidly and reversibly reduced  $\text{Ca}^{2+}$  influx through both N- and P/Q-type channels by 51% and postsynaptic responses by 78%, i.e. release was proportional to  $\text{Ca}^{2+}$  raised to the power  $\approx 2.5$ .

The weak dependence of release on changes in  $\text{Ca}^{2+}$  when channel toxins block channels suggests little overlap between  $\text{Ca}^{2+}$  microdomains from channels supporting release or substantial segregation of channel subtypes between terminals. The proportionately greater reduction of transmission by muscarinic receptors compared to  $\text{Ca}^{2+}$  channel toxins suggests that they directly affect the release machinery in addition to reducing  $\text{Ca}^{2+}$  influx. © 2001 IBRO. Published by Elsevier Science Ltd. All rights reserved.

**Key words:**  $\text{Ca}^{2+}$  channels,  $\omega$ -CTX-GVIA,  $\omega$ -Aga-IVA,  $\text{Ca}^{2+}$  imaging, muscarinic, presynaptic inhibition.

Much of our understanding of the relationship between presynaptic  $\text{Ca}^{2+}$  influx and neurotransmitter release comes from work on invertebrate synapses<sup>1–3,13,14,28–32,52,68,69</sup> and vertebrate peripheral nervous system or neuromuscular junctions.<sup>10,17,24,25,33,34,39</sup> These synapses are characteristically large (greater than a few micrometers diameter or length) and/or are situated near the surface of a muscle or ganglion, which facilitates optical recording of presynaptic  $\text{Ca}^{2+}$  influx, with simultaneous electrical

measurements of excitatory postsynaptic potentials to monitor transmitter release. In the vertebrate CNS, simultaneous pre- and postsynaptic electrophysiological measurements comparing  $\text{Ca}^{2+}$  current to release have been made,<sup>7,9,22</sup> and recently presynaptic fluorescent  $\text{Ca}^{2+}$  imaging has been combined with measurements of postsynaptic responses<sup>66</sup> at the large calyx of Held synapses.

Fluorescence-based measurements of  $\text{Ca}^{2+}$  influx into presynaptic terminals have been correlated with the strength of synaptic connections in rat brain slice preparations from the hippocampus for the CA3–CA1 and mossy fiber–CA3 synapses,<sup>42,43,47,51,63</sup> and at cerebellar parallel fiber–Purkinje cell synapses.<sup>35,44,46</sup> The preservation of the laminar axonal projections characteristic of these brain regions in slices facilitates the loading of  $\text{Ca}^{2+}$  indicators specifically into presynaptic terminals by local perfusion or injection of membrane-permeant acetoxymethyl derivatives into the space surrounding axons, so that simultaneous recording of postsynaptic field potential and spatially averaged  $\text{Ca}^{2+}$  influx from presynaptic terminals is possible.

Functional diversity is a hallmark of synaptic connections wherever comparative studies have been done, and this diversity is undoubtedly fundamental to the specific

\*Corresponding author. Present address: Department of Neuroscience, University of Calgary, 3330 Hospital Drive NW, Calgary, Alberta, Canada T2N 4N1. Tel.: +1-403-220-4488; fax: +1-403-283-2700.

E-mail address: sjmullig@ucalgary.ca (S. J. Mulligan).

**Abbreviations:** ACSF, artificial cerebrospinal fluid;  $\omega$ -Aga-IVA,  $\omega$ -agatoxin-IVA; AOB, accessory olfactory bulb; AOT, accessory olfactory tract; BAPTA, bis(2-aminophenoxy)ethane-*N,N,N',N'*-tetra-acetate;  $[\text{Ca}^{2+}]_i$ , calcium influx;  $[\text{Ca}^{2+}]_o$ , extracellular calcium concentration; CNQX, 6-cyano-7-nitroquinoxaline-2,3-dione;  $\omega$ -CTX-GVIA,  $\omega$ -conotoxin-GVIA; EGTA, ethyleneglycolbis(aminoethyl ether)tetra-acetate;  $\Delta F/F$ , change in fluorescence/baseline; FAD(H), (reduced) flavin adenine dinucleotide; HEPES, *N*-2-hydroxyethylpiperazine-*N'*-2-ethanesulfonic acid; LFP, local field potential; MCN-A-343, 4-hydroxy-2-butyl-1-trimethylammonium-*m*-chlorocarbanilate chloride; NAD(H), (reduced) nicotinamide adenine dinucleotide; VDCC, voltage-dependent calcium channel.

operations of various neural circuits. We are interested in understanding how synapses function as variable elements in complete neural circuits and how they are regulated by neuromodulatory inputs. Because of the diversity of synaptic properties, it is important to extend quantitative studies of the relationship between presynaptic  $\text{Ca}^{2+}$  and transmitter release to new synaptic connections in vertebrate nervous systems. While brain slices offer many advantages, they are not well suited to maintaining long-range axonal projections such as those originating from distant nuclei.

For this study we developed an *in vitro, en bloc* preparation consisting of the frog forebrain that offers accessibility for electrophysiological and microfluorometric recording, and for pharmacological manipulations, as in slice preparations, while leaving extended neural circuits and axonal projections intact. We took advantage of the highly specific axonal projections of the mitral cells of the accessory olfactory bulb (AOB) to the amygdala to selectively load presynaptic terminals with dextran-conjugated  $\text{Ca}^{2+}$  indicators. We have quantitatively investigated the relationship between  $\text{Ca}^{2+}$  influx and transmitter release when  $\text{Ca}^{2+}$  influx is changed by presynaptic  $\text{Ca}^{2+}$  channel blockers, reduced extracellular  $[\text{Ca}^{2+}]_o$  ( $[\text{Ca}^{2+}]_o$ ) or activation of cholinergic presynaptic receptors. We report on the relative contribution of different subtypes of presynaptic voltage-dependent calcium channels (VDCCs) to triggering transmitter release and characterize the pharmacology of presynaptic acetylcholine receptors that block voltage-dependent  $\text{Ca}^{2+}$  influx. Through our quantitative fluorometric measurements of  $\text{Ca}^{2+}$  influx, we have obtained data on the apparent cooperativity between  $\text{Ca}^{2+}$  influx and transmitter release when influx is reduced using these different conditions. We discuss the differences we observed between toxin blockade and reduced  $[\text{Ca}^{2+}]_o$  in the context of the overlap of individual  $\text{Ca}^{2+}$  channel domains for triggering release at this synapse.

## EXPERIMENTAL PROCEDURES

### *In vivo filling of mitral cell terminals with $\text{Ca}^{2+}$ indicators*

Adult male *Rana pipiens* ( $N=38$ ; Sullivan Co., Nashville, TN, USA) were used in this study. All experimental procedures were in accordance with Simon Fraser University Animal Care Use Regulations, which are in turn in line with national guidelines on the ethical use of animals. All efforts were made to minimize the number of animals used and their suffering. Frogs were anesthetized by immersion in a pH neutral 60 mg/100 ml solution of tricaine methanesulfonate (Sigma).<sup>60</sup> Frogs were removed from solution when they did not respond to a foot pinch (an adequate level of sedation was ensured throughout the surgical procedure by assessing tongue and eye withdrawal reflexes). A midline incision was made to the skin covering the hard palate beginning near the vomeronasal organ and ending at the rostral end of the soft palate. A craniotomy was performed with fine-tipped rongeurs to expose a small area of the ventral surface of the brain at the level of the AOB. The dura covering each AOB was removed with forceps and the surface carefully dried with fine tissue paper. The tips of broken micropipettes were filled with concentrated solution (10% w/v in double-deionized water or 1.5% bovine serum albumin) of dextran-conjugated fluorescent  $\text{Ca}^{2+}$  indicators or anatomical tracers. The dyes used were  $\text{Ca}^{2+}$ -Green-1 (mol. wt 3000 or 10,000), Oregon Green 488 BAPTA-1,

Fluo-4, Texas Red and Rhodamine Green (all from Molecular Probes, Eugene, OR, USA). Three to five filled micropipette tips ( $\approx 15$  nl total volume) were carefully inserted into the external plexiform layer of each AOB and dye was injected using positive air pressure. After injection, the skin flaps covering the hard palate were sutured together with No. 9-0 surgical silk. Frogs were placed in isolation, half covered with water, while they regained consciousness (usually within 2 h). They remained in isolation for one to three days to allow for sufficient intraxonal dye transport time.

### *In vitro forebrain preparation*

Tricaine methanesulfonate-anesthetized frogs were rapidly decapitated, and the brain was removed and placed in chilled ( $6^\circ\text{C}$ ) artificial cerebrospinal fluid (ACSF) containing (in mM) 72 NaCl, 26  $\text{NaHCO}_3$ , 2.5  $\text{NaH}_2\text{PO}_4$ , 0.5  $\text{Na}_2\text{HPO}_4$ , 1.5  $\text{MgSO}_4$ , 2 KCl, 2  $\text{CaCl}_2$  and 10 glucose, bubbled with carbogen gas (95%  $\text{O}_2/\text{CO}_2$ ) to pH 7.4.<sup>16</sup>

The forebrain and a portion of the diencephalon rostral to the tectum were split into two halves by cutting down the middle of the olfactory bulb and through the caudal hemispheric adhesion of the telencephalon. One forebrain hemisphere was placed in a Sylgard<sup>TM</sup>-lined recording dish milled from Lexan<sup>TM</sup>, with a main chamber for the brain (1.5 ml) and a narrow outflow path (1 ml). To expose the inner (ventricular) wall of the telencephalon, a dorsal to ventral (i.e. coronal) cut through the lateral wall of the telencephalon was made at the level of the thalamus with fine iris scissors. The dorsal margin of the telencephalon was then cut along the rostrocaudal axis and a flap of tissue comprising the dorsal two-thirds of the medial cortex was removed. The remaining tissue was secured to the Sylgard<sup>TM</sup> floor with bent minuten pins (five to 10) inserted around the tissue margin, with the ventricular surface of the lateral cortex facing upwards, taking care to avoid excessively stretching or distorting the tissue. The brain was continually perfused with carbogen-bubbled ACSF, gravity fed at a rate of 1–2 ml/min. Temperature was rigorously maintained at  $16 \pm 0.5^\circ\text{C}$  with a Peltier cooling device, monitored with a 1-mm-diameter thermistor probe (Fluke, model 51 K/J) submerged in the bath beside the brain. For reduced  $\text{Ca}^{2+}$  experiments,  $\text{Ca}^{2+}$  was replaced with equal amounts of  $\text{Mg}^{2+}$  to help maintain a constant threshold for mitral cell axon activation.

### *Stimulation*

Bipolar stimulating electrodes were made from 75- $\mu\text{m}$  enamel-coated tungsten (California Fine Wire) wire glued together with Krazy<sup>TM</sup> glue. These were placed on the fluorescently labeled accessory olfactory tract (AOT) approximately 200  $\mu\text{m}$  posterior to the AOB. Stimulus pulses of 10–500  $\mu\text{A}$  at a constant 200- $\mu\text{s}$  duration were delivered to the AOT with a pulse generator and isolation unit (PG4000, SIU90, Neurodata Instruments). For experiments where the effects of decreased  $\text{Ca}^{2+}$  or drug application were studied, the stimulation intensity was set to 20% above the threshold for maximum evoked optical and field responses. The standard experimental protocol consisted of either a single pulse or short trains of pulses (100 ms interpulse interval) delivered once every 5 min.

### *Electrophysiological recording*

Local field potentials (LFPs) were recorded in response to electrical stimulation with low-resistance (impedance  $<2$  M $\Omega$ ) ACSF-filled glass microelectrodes. Typically, recordings were made from the AOT, half way between the AOB and the amygdala, to record the presynaptic volley, and in the amygdala to record the evoked postsynaptic response. The electrode in the amygdala was positioned approximately 250  $\mu\text{m}$  below the ventricular surface to maximize the amplitude of the negative phase of the synaptically evoked field potential. Using the dye fluorescence as a guide, the electrode on the AOT was positioned superficially to maximize the amplitude of the presynaptic volley component of the evoked field potentials, but at the same time minimize damage to the mitral cell axons. The amygdala LFPs

were amplified 1000 times and bandpass filtered between 0.1 Hz and 1 kHz. The AOT field potentials were amplified 1000 times and bandpass filtered between 0.1 Hz and 10 kHz (SR590 Stanford Research Systems). Conditioned signals were digitized at a rate of 5000 samples per second with a 12-bit A/D board (MacADIO II) and acquired with a microcomputer (Macintosh Quadra 800) using Superscope-II™ software (GW Instruments, Cambridge, MA, USA). Off-line analysis was performed using commercial software (Igor™ Wavemetrics, Eugene, OR, USA).

Whole-cell recordings from amygdala neurons were obtained using pipettes containing 85 mM potassium gluconate, 4 mM KCl, 4 mM NaCl, 5 mM D-glucose, 5 mM HEPES, 500 μM glutathione, 2 mM MgCl<sub>2</sub>, 1 mM ATP, 300 μM GTP and 1 mM EGTA. Access resistances were 25–40 MΩ at the start of recording and cells were rejected if the access exceeded 50 MΩ before 10 min of carbachol application. Holding potential was –60 to –65 mV. Pipette resistances were 8–12 MΩ. Rhodamine Green Dextran (Molecular Probes, Eugene, OR, USA) was applied to the AOB *in vivo* 18–36 h prior to recording, to label the AOT and terminals in the amygdala to facilitate placement of the stimulating electrode on the AOT and to guide placement of the whole-cell and LFP recording pipettes in the amygdala. Amygdala neurons receiving monosynaptic connections from AOT fibers were selected on the basis of a short and constant latency to onset of the excitatory postsynaptic current during repetitive firing, as well as a continuously graded excitatory postsynaptic current amplitude with increasing stimulus intensity. Forty-five per cent (5/12) of neurons for which successful whole-cell recordings were obtained met all these criteria.

#### Microfluorimetry

High-temporal-resolution measurements of presynaptic Ca<sup>2+</sup> transients were taken using a custom-built epifluorescence microscope. Excitation light from either a stabilized 150-W xenon lamp (OptiQuip, Highland Mills, NY, USA) or a 50-W tungsten lamp was delivered to the specimen in the form of an aperture-limited spot. Light from the arc lamp was attenuated 25–50% to reduce dye fading. A filter set (Chroma Corporation, Brattleboro, VT, USA) consisting of a dichroic beamsplitter (DCLP 505LP) and fluorescence excitation (488 ± 10 nm) and emission (535 ± 25 nm) filters was used. A ×20 or ×40 water immersion objective lens (Olympus LUMPlanFI) was used to image the filled terminals and focus the fluorescence signals generated from a 200-μm-diameter illumination spot in the center of the amygdala onto a photomultiplier tube (Hamamatsu, model H5783). The photomultiplier output was filtered (d.c., 300 Hz) with a custom amplifier before being digitized and acquired with a microcomputer. When terminals were filled with Ca<sup>2+</sup>-Green-dextran or Oregon Green 488 BAPTA-1-dextran, the large signal-to-noise ratio of the fluorescence changes eliminated the need for digital filtering or smoothing of data. For some measurements, fluorescence signals were converted to ΔF/F, where F is the fluorescence before the stimulus corrected by subtracting a measurement of tissue autofluorescence taken from an identically sized illumination spot positioned over tissue adjacent to the stained terminals, and ΔF is the change in fluorescence. Background autofluorescence was typically 20–40% of the total fluorescence with Ca<sup>2+</sup>-Green or Oregon Green 488 BAPTA-1, whereas with Fluo-4-dextran tissue fluorescence was several times greater than the dye fluorescence, making it impossible to accurately estimate a ΔF/F value. Because we kept our illumination intensity low, dye bleaching was negligible, as evidenced by a constant resting fluorescence intensity throughout the experiment.

#### Quantification of local field potential and fluorescence signals

The magnitude of the postsynaptic response was defined as the amplitude of the negative peak of the amygdala LFP waveform. The AOT LFP recording consisted of a characteristic presynaptic volley waveform,<sup>19</sup> with some contamination from delayed postsynaptic currents. Therefore, only the size and shape of the first positive peak amplitude from baseline were used as a measure of AOT activation. Despite a constant amplitude for the AOT volley

and the afferent volley component of the AOB LFP, two closely timed stimulation pulses delivered to the AOT produced fluorescence transients in the amygdala, the second of which was smaller than the first, when the presynaptic terminals were loaded with high-affinity Ca<sup>2+</sup> indicators such as Ca<sup>2+</sup>-Green-1-dextran (K<sub>d</sub> 260 nM) or Oregon Green 488 BAPTA-1-dextran (K<sub>d</sub> 340 nM; Fig. 2A, B). However, when terminals were loaded with the low-affinity Ca<sup>2+</sup> indicator Fluo-4-dextran (K<sub>d</sub> estimated at 3.8 μM by Molecular Probes), a constant incremental change in fluorescence was seen with repeated stimulation of the AOT (Fig. 2C). This indicates that partial saturation of the high-affinity dyes was responsible for the ΔF/F decrements and enabled us to calculate the Ca<sup>2+</sup> influx per action potential and quantify changes in intracellular Ca<sup>2+</sup> influx (Δ[Ca<sup>2+</sup>]<sub>i</sub>) using the following formula:<sup>21</sup>

$$\Delta[\text{Ca}^{2+}]_i = ([\text{Ca}^{2+}]_o + K_d)(1 - \alpha)/2\alpha,$$

where  $\alpha = (F_3 - F_2)/(F_1 - F_0)$  and [Ca<sup>2+</sup>]<sub>o</sub> is the resting Ca<sup>2+</sup> concentration, which for our study we estimated to be 50 nM, K<sub>d</sub> is the equilibrium dissociation constant of the indicator, F<sub>0</sub> is the indicator fluorescence at resting [Ca<sup>2+</sup>]<sub>o</sub>, F<sub>1</sub> is the peak fluorescence produced by the first action potential, F<sub>2</sub> is the fluorescence immediately before the second action potential and F<sub>3</sub> is the peak fluorescence produced by the second action potential. Use of this equation to estimate Δ[Ca<sup>2+</sup>]<sub>i</sub> assumes that the influxes produced by each action potential are the same and that the decay in [Ca<sup>2+</sup>]<sub>i</sub> between action potentials is small compared with the peak [Ca<sup>2+</sup>]<sub>i</sub>,<sup>21</sup> as confirmed by our Fluo-4 and AOT LFP recordings.

Statistical analysis was done using an independent group *t*-test (two-tailed); significance was achieved when *P* < 0.01.

#### Anatomical characterization of dye-filled structures

AOBs were injected with the dextran-conjugated fluorescent indicators Texas Red or Rhodamine Green (Molecular Probes) and dissected as described above. Brains were transferred to the cavity of a depression slide and secured in place with a Cell Tac™-coated microscope slide. A ×60 water immersion objective lens (Olympus LUMPlanFI) was used to image the filled structures. Images were made with a Zeiss LSM 410 confocal microscope using the 568-nm laser line (96.8% attenuation), a dichroic beamsplitter (580 nm), an emission filter (610 nm LP) and standard acquisition software.

#### Drugs and their delivery

For all experiments except those in which Ca<sup>2+</sup> channel blockers were applied, carbogen (95%/5% O<sub>2</sub>/CO<sub>2</sub>)-bubbled ACSF was flowed over the brain through a gravity-fed system (saline drips; Baxter) at a rate of 1–2 ml/min. A four-way manual valve located near the preparation was used to switch between different solutions. Experiments with the Ca<sup>2+</sup> channel blockers ω-conotoxin-GVIA (ω-CTX-GVIA) and ω-agatoxin-IVA (ω-Aga-IVA) (Alamone Labs, Israel) were performed in a static bath. For these experiments, perfusion with ACSF was stopped and oxygen and pH levels were maintained by directly bubbling the fluid in the chamber with carbogen. The gas mixture was delivered via a ring of plastic tubing embedded in the Sylgard™ lining the bottom around the periphery of the main chamber of the dish. Pinholes (10–20) in the wall of the plastic tubing created a sprinkler-type bubbling, the rate of which was controlled by a manual valve. It was possible to make both optical and electrophysiological measurements during direct bubbling of the bath using water immersion lenses. The physiological stability of preparations in the static bath was carefully examined in several control experiments; the evoked field and optical responses were stable over the course of several hours. Stock solutions of the peptide toxins ω-CTX-GVIA and ω-Aga-IVA were prepared in distilled water, divided into 100-μl aliquots and stored at –80°C until used. These stock solutions were added to the bath to final concentrations of: ω-CTX-GVIA, 1 μM; ω-Aga-IVA, 200 nM. Aliquots (100 μl) of the other concentrated drug solutions used were kept at –20°C. Aliquots were added to 100 ml ACSF superfusing the preparation. Final drug concentrations were: nifedipine, 10–50 μM; carbachol (Sigma), 10–200 μM;

6-cyano-7-nitroquinoxaline-2,3-dione (CNQX), 10  $\mu\text{M}$ ; 2-amino-5-phosphovaleric acid (Precision Biochemicals, N. Vancouver, Canada), 100–150  $\mu\text{M}$ ; nicotine, 10–50  $\mu\text{M}$ ; scopolamine, 100  $\mu\text{M}$ ; MCN-A-343, 100–600  $\mu\text{M}$ ; 4-diphenylacetoxy-*N*-(2-chloroethyl)-piperidine hydrochloride (RBI-Sigma), 100  $\mu\text{M}$ ; mibefradil (gift from Roche Pharmaceuticals), 10–50  $\mu\text{M}$ .

## RESULTS

### *Loading terminals with $\text{Ca}^{2+}$ indicator and quantitative measurements of $\text{Ca}^{2+}$ influx and transmitter release*

The anatomy of the frog AOB is similar to the main olfactory bulb, but is less organized and laminar.<sup>26</sup> Unlike the main olfactory bulb, which has diffuse mitral cell axonal projections to the telencephalon, the mitral cells of the AOB project exclusively to the amygdala.<sup>48,49</sup> The well-defined AOT emerges from the posterior face of the AOB and courses posteriorly for 2–3 mm along the ventromedial wall of the lateral cortex to terminate in the amygdala. Neuronal somata in the amygdala projecting back to the AOB were not observed, as reported previously.<sup>49</sup> A lateral view of the frog brain is illustrated in Fig. 1A, showing the injection site for the  $\text{Ca}^{2+}$  indicators into the AOB and the mitral cell projections from the AOB to the amygdala. Application of dextran-conjugated dyes to the AOB filled numerous somata and their dendrites in the AOB and a large terminal field in the amygdala (Fig. 1B). One to seven days after the injection, all stained somata appeared healthy, with no evidence of dye sequestration, and their dendrites were completely filled and unblebbed (Fig. 1C).

A single, maximal stimulus of the AOT produced a peak background corrected  $\Delta F/F$  of  $82.3 \pm 7.1\%$  ( $N=26$ ; range: 30–180%). This transient reached a peak 10–25 ms after onset and the recovery could be fitted reasonably well by a single exponential with a time constant of 0.9–2 s. Neither the rate of transient recovery nor the peak amplitude was correlated, nor were they significantly affected by intra-axonal dye transport time (one to seven days), suggesting that there were not large variations in the  $\text{Ca}^{2+}$  buffering by the indicator between preparations. The recovery rate of transients for terminals filled with the low-affinity indicator Fluo-4-dextran were 160 and 180 ms in two separate experiments, suggesting that loading with the high-affinity indicator affected the apparent rate of recovery.<sup>35</sup>

Images of a  $\text{Ca}^{2+}$ -Green-1-loaded preparation visualized via the ventricular surface of one telencephalic hemisphere using a low-magnification objective lens ( $\times 4$ ) are presented in Fig. 1B, illustrating the fluorescence change resulting from 20 action potentials stimulated at a rate of 10 per second. Fluorescence increases were clearly seen in the mitral cell axons in the AOT as well as the terminal field in the amygdala, so a more detailed anatomical examination was undertaken to determine the source of fluorescence signals within the amygdala and the fiber tract. Fibers projecting into the AOB (other than the primary sensory fibers from the vomeronasal organ) have not been observed in the frog<sup>49</sup> and, as expected, retrogradely filled neuronal somata outside the AOB were not seen after application of

dextran-conjugated dyes into the AOB. A stack of two-photon laser scanning microscope images of somata and dendrites of mainly mitral cells is shown in Fig. 1C, with some granule cells within the AOB in a live preparation. The fasciculated tract of the mitral cell axons exhibited a few *en passant*, knob-like enlargements, that may or may not be isolated synaptic boutons, as it coursed along the inner wall of the telencephalon en route to the amygdala (Fig. 1D). This finding is consistent with the study of Scalia *et al.*,<sup>49</sup> and suggests that there is little synaptic interaction with neurons of the lateral cortex before reaching the amygdala. Examination of the fluorescence within the amygdala by confocal microscopy indicated that the majority of the signal originated from a dense compact web of serial and terminal boutons (Fig. 1E), with a small contribution from very thin preterminal axons. All quantitative measurements of the fluorescence changes from presynaptic terminals were taken from an aperture-limited illumination spot ( $\sim 200 \mu\text{m}$ ) in the center of the amygdala, where the preterminal axonal contribution to total fluorescence was expected to be minimal. Presynaptic terminals ranged from 1 to 3  $\mu\text{m}$  in diameter, with an average size of approximately 1.5  $\mu\text{m}$  (Fig. 1F). Terminals were often found in “grape-like” clusters within the amygdala (Fig. 1G) and as serial boutons along thin axons (Fig. 1H). This average terminal size is slightly larger than the average terminal size ( $\leq 1 \mu\text{m}$ ) typically reported in other vertebrate brain regions, with the exception of the mossy fiber terminals in the hippocampal CA3 region, where the average terminal size is 3–6  $\mu\text{m}$ .<sup>12</sup> It has been estimated that presynaptic terminals make up approximately 75% of the volume of parallel fibers in the cerebellum<sup>37</sup> and similarly provide 75% of the fluorescence in the mossy fiber–CA3 synaptic region.<sup>35</sup> Mitral cell terminals in the amygdala are numerous and their diameter is large relative to the sparse thin axons, and therefore we estimate that terminal contribution to the fluorescent signal is at least equal to, and probably greater than, that reported for the cerebellum and hippocampus.

Dextran-conjugated  $\text{Ca}^{2+}$  indicators are excellent retrograde and anterograde tracers that do not leak out of neurons or become sequestered in internal compartments during the *in vivo* transport period.<sup>36</sup> However, due to the long intra-axonal dye transport time, there was a small possibility that some of the dye may have been released from the presynaptic terminals and taken up by neurons in the amygdala through endocytotic processes.<sup>67</sup> Postsynaptic responses were blocked with 10  $\mu\text{M}$  CNQX to verify that the fluorescence changes observed in the amygdala were due to presynaptic and not postsynaptic  $\text{Ca}^{2+}$  influx. Blockade of postsynaptic receptors had no effect on the stimulus-evoked fluorescence changes (Fig. 2). The addition of the *N*-methyl-D-aspartate receptor antagonist 2-amino-5-phosphovaleric acid (100–150  $\mu\text{M}$ ) did not produce further decrement to the amygdala LFP ( $N=3$ ; data not shown) or the fluorescence transient. This indicates that  $\text{Ca}^{2+}$  influx into presynaptic, not postsynaptic, structures was responsible for the fluorescence transients, and that the postsynaptic current was mainly due to activation of

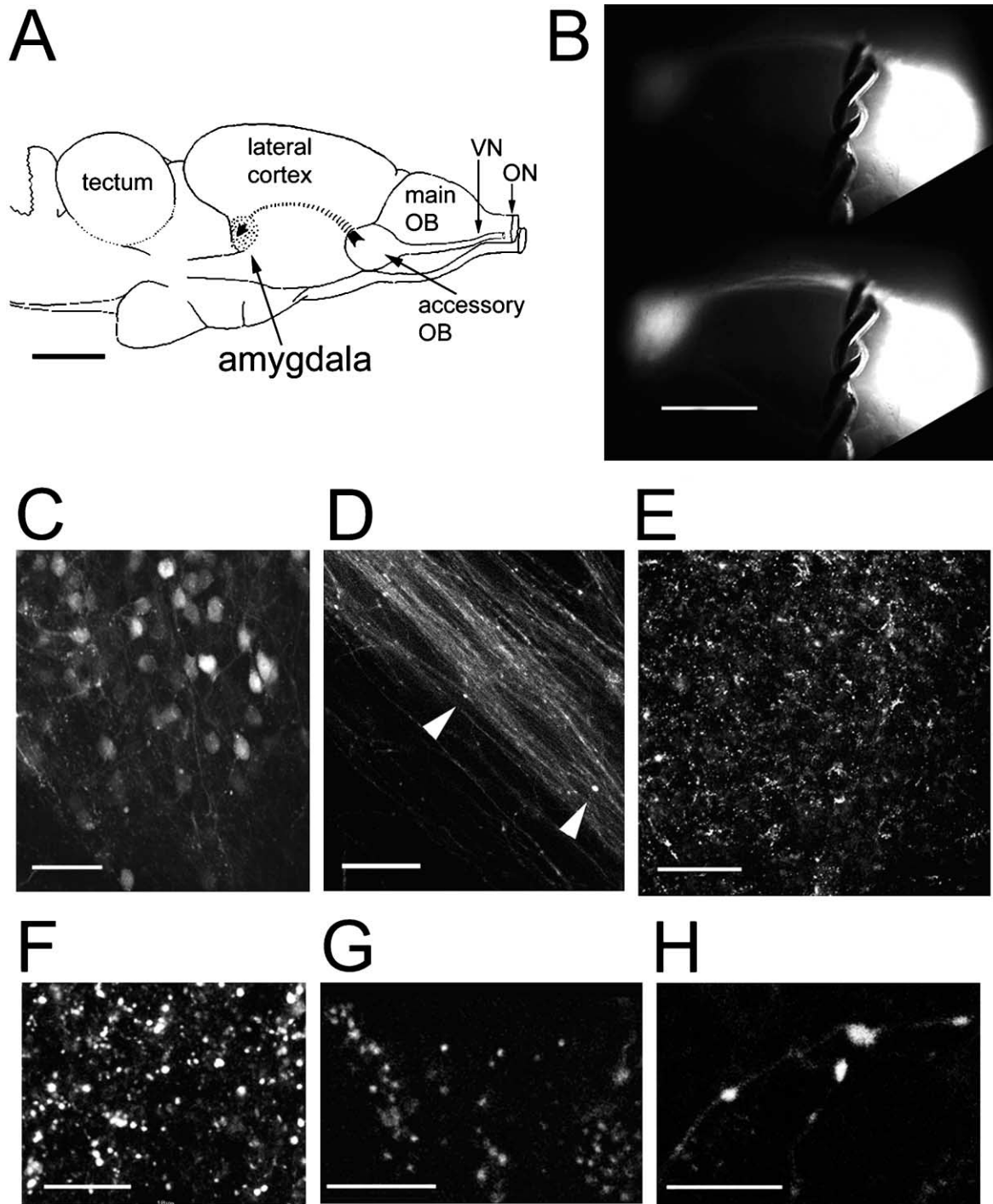


Fig. 1. The projection of the AOB to the amygdala in frog. (A) Sketch of the right side of the brain of *R. pipiens* showing the accessory olfactory pathway. OB, olfactory bulb; ON, olfactory nerve; VN, vomeronasal nerve. Adapted from Scalia.<sup>48</sup> (B) A low-power ( $\times 4$ ) CCD image of the mitral cell projection from the AOB to the amygdala as viewed from the ventricular surface of the lateral cortex shows the fluorescence level of the unstimulated pathway (above) and the stimulated pathway (below). (C) A two-photon image taken near the center of the AOB shows the dye-filled somata and dendrites of the mitral and granule cells. (D) Confocal microscope image ( $1.2\ \mu\text{m}$  thick) of the AOT fibers taken approximately  $200\ \mu\text{m}$  outside the amygdala, showing few synaptic boutons (arrows). (E) Confocal microscope stack of three images ( $10\ \mu\text{m}$  total thickness) taken from the center of the amygdala shows the density of the mitral cell terminal field. (F–H) At higher magnification, a stack of 20 images (F;  $22\ \mu\text{m}$  total thickness) reveals the typical size of the terminals that were commonly found in grape-like clusterings (G), but also boutons along thin axons (H). G and H are single images  $1.2\ \mu\text{m}$  thick. Scale bars =  $1\ \text{mm}$  (A, B),  $25\ \mu\text{m}$  (C, D, F),  $100\ \mu\text{m}$  (E),  $20\ \mu\text{m}$  (G),  $10\ \mu\text{m}$  (H).

$\alpha$ -amino-3-hydroxy-5-methyl-4-isoxazolepropionate-type glutamate receptors.

To show that the measurements taken from the

amygdala were the result of AOT stimulation and not stimulation of cortical associational fibers in close proximity, the stimulation electrode was moved off the

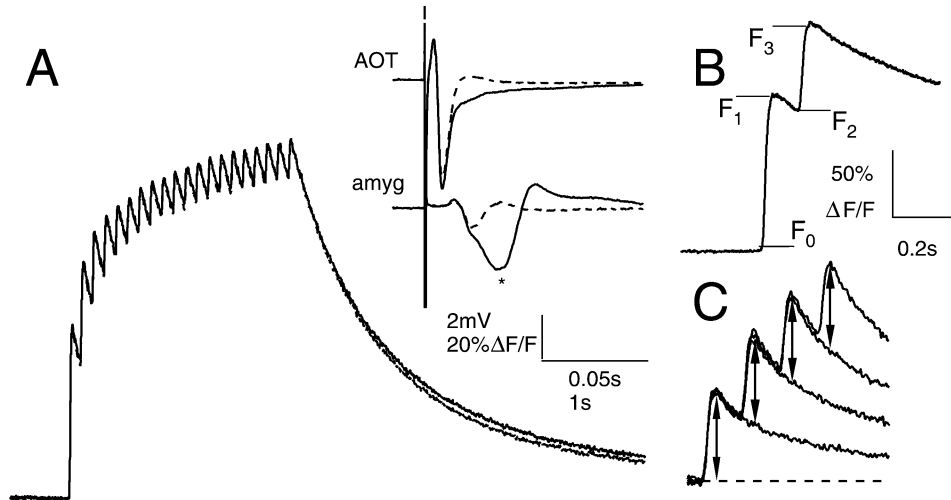


Fig. 2. Fluorescent changes in the amygdala are the result of  $\text{Ca}^{2+}$  influx into mitral cell presynaptic terminals. (A) A typical experiment showing that the fluorescence changes ( $\Delta F/F$ ) and the AOT volley response remain virtually unchanged, while only the presynaptic volley component of the amygdala LFP remains after a 20-pulse, 10-Hz stimulus train is applied to the AOT in ACSF and 30 min in  $10 \mu\text{M}$  CNQX. (Amygdala projections were loaded with the high-affinity  $\text{Ca}^{2+}$  indicator  $\text{Ca}^{2+}$ -Green-1.) The size and shape of the first positive peak amplitude from baseline of the AOT field was not contaminated by postsynaptic currents and was therefore used to measure AOT activation. The asterisk on the amygdala LFP inset marks the point used to measure postsynaptic activation strength. Fluorescence transients are individual recordings, AOT and amygdala LFPs are averages of 16 responses. (B) The fluorescence levels used to define  $\alpha = (F_3 - F_2)/(F_1 - F_0)$  in brains loaded with the high-affinity  $\text{Ca}^{2+}$  indicators. Single trace (Oregon Green 488 BAPTA-1). (C) Fluorescent transients from a brain loaded with the low-affinity  $\text{Ca}^{2+}$  indicator Fluo-4. Each stimulus pulse produces the same incremental change in fluorescence, indicating the same change in  $\text{Ca}^{2+}$  influx per action potential.

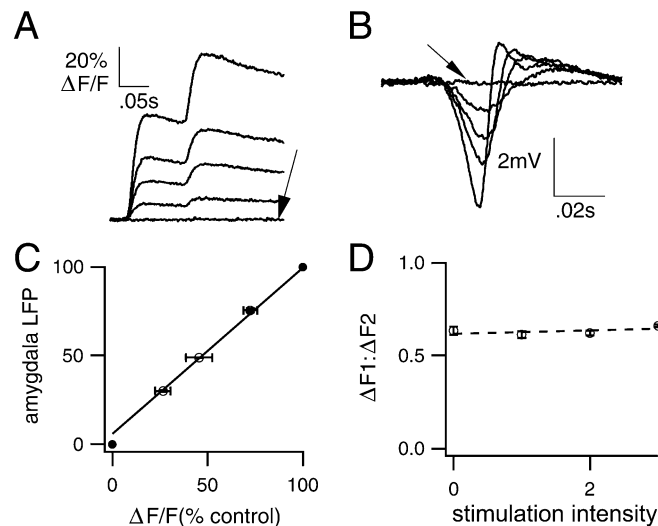


Fig. 3. The presynaptic  $\text{Ca}^{2+}$  transient amplitude increases linearly with the amygdala LFP. (A, B) The  $\text{Ca}^{2+}$  transient (A) and amygdala LFP (B) recordings show baseline responses (arrows) to a suprathreshold stimulus applied to a site adjacent to the AOT ( $<100 \mu\text{m}$ ), but increased stimulation intensity applied to the AOT increases the  $\text{Ca}^{2+}$  transient and amygdala LFP responses (individual recordings in A and B). (C, D) The  $\text{Ca}^{2+}$  transient increases linearly with the amplitude of the amygdala LFP, while the ratio of the first to second  $\text{Ca}^{2+}$  transients ( $\Delta F_1 : \Delta F_2$ ) remained constant ( $N=3$ ; stimulation intensity is arbitrary units).

fluorescently labeled AOT approximately  $100 \mu\text{m}$  towards either the dorsal or the ventral margin and a suprathreshold stimulus applied. Neither a  $\text{Ca}^{2+}$  transient nor an LFP response was observed in the amygdala (Fig. 3).

With the stimulation electrode placed on the AOT and the stimulation intensity increased incrementally, the presynaptic  $\text{Ca}^{2+}$  transient amplitude increased linearly with the increase in the amygdala LFP response, while the ratio of the first to second  $\text{Ca}^{2+}$  transients remained

constant (Fig. 3C, D). The constancy of the  $F_1 : F_2$  ratio indicated that increasing stimulus strength recruited more presynaptic fibers, but did not increase the amount of  $\text{Ca}^{2+}$  influx per action potential. It also confirmed the results of the ionotropic glutamate blocking experiments, which indicated that there was no postsynaptic contribution to the fluorescence transients.

Repeated suprathreshold stimulation of the AOT in preparations loaded with high-affinity  $\text{Ca}^{2+}$  indicators ( $\text{Ca}^{2+}$ -Green-1 and Oregon Green 488 BAPTA-1)

produced a build-up in fluorescence, during which each subsequent fluorescence transient was smaller than that of the previous one (Fig. 2A, B). The qualitative characteristics of the build-up of fluorescence are similar to those measured from presynaptic terminals in other preparations.<sup>21,43,56</sup> Both the axonal volley recorded from the AOT and the presynaptic volley component of the LFP in the amygdala indicated that the number of stimulated axons did not change during action potential trains. In preparations where the presynaptic terminals were loaded with the low-affinity  $\text{Ca}^{2+}$  indicator Fluo-4 (Fig. 2C), decrements in  $\Delta F/F$  with each successive stimulus in a short train were not seen. These two findings indicate that it is reasonable to conclude that the influx of  $\text{Ca}^{2+}$  induced by each of a pair of action potentials was the same, so the decrement in  $\Delta F/F$  to successive action potentials that was seen with high-affinity  $\text{Ca}^{2+}$  is proportional to the degree of saturation of the indicator. This saturation phenomenon enabled us to estimate the  $\text{Ca}^{2+}$  influx per action potential as  $62.0 \pm 4.0$  nM (26 preparations) and quantify changes in  $\text{Ca}^{2+}$  influx using the paired-pulse dye saturation methodology developed by Feller *et al.*<sup>21</sup> (see Experimental Procedures). There are two major advantages of this method for estimating  $\Delta[\text{Ca}^{2+}]$ . First, unlike methods based on calculating  $\Delta F/F$ , dye fading or changes in axonal excitability during the experiment will not affect the ratio of  $\Delta F_1$  to  $\Delta F_2$ . Fewer stimulated boutons will decrease the magnitude of  $\Delta F$  equally for the first and second pulses, leaving the  $\Delta F_1 : \Delta F_2$  ratio unchanged (Fig. 3C, D), whereas a reduction in influx will reduce the  $[\text{Ca}^{2+}]$  reached by the first stimulus and hence result in a proportionately larger  $\Delta F/F$  to the second pulse, i.e. the ratio will be closer to 1. This is important under conditions such as those of this study, where a decrease in  $\Delta F/F$  in response to a stimulus delivered to the AOT could be due to either less  $\text{Ca}^{2+}$  influx per presynaptic bouton or fewer boutons exhibiting any influx. Also, although changes in background tissue fluorescence resulting from production, depletion or fading of fluorescent metabolites, e.g. FAD/FADH and NAD/NADH, will change total fluorescence, they will not affect the  $\Delta F_2 : \Delta F_1$  ratio.

The quantitative estimate of  $\Delta[\text{Ca}^{2+}]$  from each action potential depends upon assumptions regarding the resting  $[\text{Ca}^{2+}]$  and the  $K_d$ . Errors in estimating the absolute value of resting  $[\text{Ca}^{2+}]$  will not affect the relative comparison of  $\Delta[\text{Ca}^{2+}]$  between two times or treatments, but changes in resting  $[\text{Ca}^{2+}]$  during the experiment will lead to errors. Fortunately, the effect of changes in resting  $[\text{Ca}^{2+}]$  to the estimate of  $\Delta[\text{Ca}^{2+}]$  are small if  $K_d > \text{resting } [\text{Ca}^{2+}]$ , which is probably the case here, since the  $K_d$  of  $\text{Ca}^{2+}$ -Green-1-dextran used in this study was around 260 nM in 100 mM KCl and for Oregon Green 488 BAPTA-1 the  $K_d$  was around 380 nM, values that are hundreds of nanomoles greater than typical estimates of resting  $[\text{Ca}^{2+}]$  in vertebrate neurons *in situ*. Furthermore, in our experiments, including those in which toxins or carbachol were applied, there was little evidence for changes in resting  $[\text{Ca}^{2+}]$ , since background subtracted values of  $F$  were stable to within 5–10% over the course of many hours.

### Reduced calcium influx and transmitter release

Having established that we could estimate the change in  $[\text{Ca}^{2+}]_i$  resulting from an action potential invading the terminals, we set about using our techniques to measure the relationship between  $\text{Ca}^{2+}$  influx and release under various conditions. Our aim was to compare the  $\text{Ca}^{2+}$ -release function when  $\text{Ca}^{2+}$  influx was varied by (i) decreasing the flux per channel with a constant number of open channels and (ii) decreasing the number of open channels while maintaining a constant flux per channel. Specifically, we were interested in whether different VDCC subtypes were present, whether all subtypes contributed to transmitter release equally and whether there was evidence for cooperativity, i.e. domain overlap, between VDCCs in stimulating release. Once these relationships had been established, we examined the effects of carbachol on  $\text{Ca}^{2+}$  influx and transmission in an attempt to determine to what extent regulation of  $\text{Ca}^{2+}$  influx was responsible for its actions.

We first reduced influx by lowering  $[\text{Ca}^{2+}]_o$ . This manipulation reduces the total influx into the terminal by reducing the flux per open channel in a manner that does not discriminate between different types of  $\text{Ca}^{2+}$  channels. At numerous vertebrate CNS synapses, a highly non-linear relationship (2.5–4) between  $\text{Ca}^{2+}$  influx and transmitter release has been seen when  $[\text{Ca}^{2+}]_o$  is reduced.<sup>8,21,44,45,55,63</sup> Typical fluorescence transients and amygdala LFP responses from an experiment where the terminals were bathed in 2, 1.5, 1 and 0.5 mM  $[\text{Ca}^{2+}]_o$  are shown in Fig. 4A and B, respectively. Reducing  $[\text{Ca}^{2+}]_o$  decreased the evoked  $\text{Ca}^{2+}$  transients and amygdala LFP responses, but did not change the amplitude or shape of the AOT volley recorded in either the AOT or the amygdala (see asterisk in Fig. 4B). The relationship between  $\text{Ca}^{2+}$  influx and  $[\text{Ca}^{2+}]_o$  was approximately linear (Fig. 4C), showing only a little saturation at higher  $[\text{Ca}^{2+}]_o$ . As has been observed at numerous synapses, the relationship between the amygdala LFP and presynaptic  $\text{Ca}^{2+}$  influx was found to be highly non-linear when  $[\text{Ca}^{2+}]$  was low (Fig. 4B), and can be described by the equation:  $\text{LFP} = k([\text{Ca}^{2+}]_i)^n$ , where LFP is the amygdala LFP response,  $[\text{Ca}^{2+}]_i$  is the spatially averaged  $\text{Ca}^{2+}$  influx,  $n$  is the order for dependence of the amygdala LFP upon  $\text{Ca}^{2+}$  influx and  $k$  is a scaling constant. Fitting a linear regression to the values obtained for log LFP amplitude vs log change in Ca influx over the range 0.5–1.5 mM  $[\text{Ca}^{2+}]_o$ , a strong non-linearity between  $\text{Ca}^{2+}$  influx and release was evident ( $n = 3.67 \pm 0.43$ ; six experiments), while between 1.5 and 2 mM, synaptic strength release was less sensitive to changes in  $\text{Ca}^{2+}$  influx. This low sensitivity to changes in  $\text{Ca}^{2+}$  influx has been seen at other synapses measured in this way, and probably represents saturation of transmitter release or postsynaptic receptors.<sup>35,59,66</sup>

### Presynaptic $\text{Ca}^{2+}$ channel pharmacology and neurotransmitter release

Numerous studies with many different kinds of synapses from both vertebrate and invertebrate preparations have confirmed variability in presynaptic VDCC

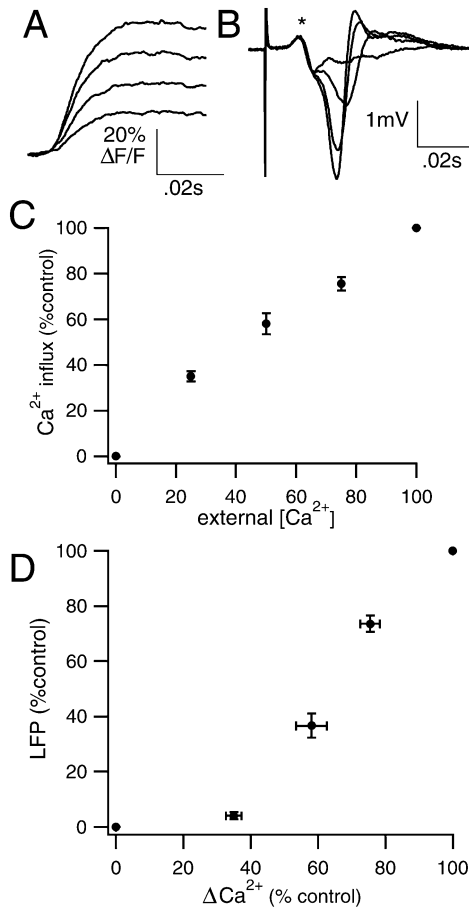


Fig. 4. Reduced  $[Ca^{2+}]_o$  and the relationship between presynaptic  $Ca^{2+}$  influx and amygdala LFP. The fluorescence (A) and the amygdala LFP (B) changes recorded during an experiment in 2, 1.5, 1 and 0.5 mM  $[Ca^{2+}]_o$ . Each trace in is the average of three or four recordings after a stable baseline was reached at each concentration (asterisk indicates the unchanging presynaptic volley component of the amygdala LFP). The dependence of the  $Ca^{2+}$  transient on  $[Ca^{2+}]_o$  is linear (C), while the relationship between the amygdala LFP and presynaptic  $Ca^{2+}$  influx is highly non-linear (D). Points on graphs C and D represent the mean  $\pm$  S.E.M. ( $N=6$ ).

expression in presynaptic terminals, both between species and from different regions within the same species.<sup>57,58</sup> We performed experiments using selective  $Ca^{2+}$  channel blockers to identify the particular channel subtypes that mediate  $Ca^{2+}$  influx and to specifically identify how different channel subtypes contribute to the release process. The fluorescence transients, amygdala LFP responses and the time course from typical experiments before and after the addition of toxins are shown in Fig. 5. Application of the N-type channel blocker,  $\omega$ -CTX-GVIA (1  $\mu$ M), caused a substantial decrement in the  $Ca^{2+}$  influx and amygdala LFP, while the presynaptic volley remained unchanged (Fig. 5A). The evoked  $Ca^{2+}$  influx was reduced by  $77.2 \pm 3\%$  and the amygdala LFP by  $88.2 \pm 3.4\%$  ( $N=5$ ) of control (Fig. 6A, B). Treatment with 200 nM  $\omega$ -Aga-IVA reduced the evoked  $Ca^{2+}$  influx by  $18.8 \pm 2.4\%$  and the amygdala LFP by  $25.2 \pm 3.1\%$  ( $N=5$ ) of control (Fig. 6A, B). The L-type  $Ca^{2+}$  channel blocker nifedipine (10–50  $\mu$ M) did not affect the  $Ca^{2+}$  transient ( $99.5 \pm 3.3\%$ ,

mean  $\pm$  S.E.M.;  $N=4$ ) or the amygdala LFP ( $101.6 \pm 4\%$ ;  $N=4$ ). In the presence of the T-type blocker mibefradil (10–50  $\mu$ M), the  $Ca^{2+}$  transient was  $100 \pm 0.3\%$  ( $N=3$ ) and the amygdala LFP remained unchanged ( $102 \pm 4\%$ ;  $N=3$ ).

It was not possible to use a range of toxin concentrations in a single experiment to determine a dose dependence for presynaptic  $Ca^{2+}$  channel block by  $\omega$ -CTX-GVIA or  $\omega$ -Aga-IVA because the block of  $Ca^{2+}$  influx was slow in onset and required up to an hour to reach steady state with 1  $\mu$ M toxin. Some of this delay is likely to reflect poor access of the toxins to presynaptic channels, either because some of these structures are deep in the tissue<sup>35</sup> and/or because channels are sequestered within narrow synaptic clefts. At a lower concentration of  $\omega$ -CTX-GVIA (500 nM), the block of presynaptic  $Ca^{2+}$  influx was even slower; nevertheless, an equivalent level of block was reached after more than an hour, confirming that 1  $\mu$ M  $\omega$ -CTX-GVIA was a saturating concentration (data not shown). Doubling the concentration of  $\omega$ -Aga-IVA had no additional effect, confirming that a 200 nM concentration produced a saturating block of the  $Ca^{2+}$  channels. Prolonged washing, up to 1 h, with ACSF did not relieve the block by  $\omega$ -CTX-GVIA or  $\omega$ -Aga-IVA.

Data comparing the decrease in  $Ca^{2+}$  influx and corresponding decrease in LFP for all manipulations (toxins, reduced  $[Ca^{2+}]_o$  and carbachol application) are summarized in Fig. 6C. When the  $Ca^{2+}$  channels were blocked by  $\omega$ -Aga-IVA, the relationship between  $Ca^{2+}$  influx and release was moderate and only slightly non-linear, i.e.  $n=1.49 \pm 0.28$ , in the convention of  $Release = k([Ca^{2+}]_o)^n$ . Since the block of  $Ca^{2+}$  influx by  $\omega$ -Aga-IVA was small enough that it mostly occurred in the range where transmission appeared to be partially saturated, i.e. equivalent to decreasing  $[Ca^{2+}]_o$  by 20%, we regard this as a minimum estimate of the cooperativity between  $\omega$ -Aga-IVA sensitive  $Ca^{2+}$  influx and release.

$\omega$ -CTX-GVIA blocks a large proportion of the  $Ca^{2+}$  influx relative to its effect on transmission. On the basis of reducing total  $Ca^{2+}$  influx, it appears to be significantly less effective at reducing synaptic strength compared to a reduction in  $Ca^{2+}$  influx achieved by reducing  $[Ca^{2+}]_o$ . The order for the dependence of release on  $Ca^{2+}$  influx was calculated to be  $n=1.44 \pm 0.11$  (five experiments), normalizing to transmission in the presence of 100%  $[Ca^{2+}]_o$  or about 1.5 if one calculates the relationship between reduced  $[Ca^{2+}]_o$  and release normalizing to release with 75%  $[Ca^{2+}]_o$  (Fig. 6C).

This observation of an only slightly non-linear relationship between  $\omega$ -CTX-GVIA-dependent  $Ca^{2+}$  influx and release (i.e.  $n < 2$ ) is in agreement with observations at the frog retinotectal synapse<sup>21</sup> and the mammalian calyx synapse,<sup>66</sup> but not as reported at hippocampal or cerebellar synapses.<sup>35,64</sup>

The  $Ca^{2+}$  channel toxins  $\omega$ -CTX-GVIA and  $\omega$ -Aga-IVA were co-applied to determine whether they targeted separate populations of presynaptic  $Ca^{2+}$  channels. The co-applied toxins greatly reduced the evoked fluorescence transient and amygdala LFP, while the presynaptic

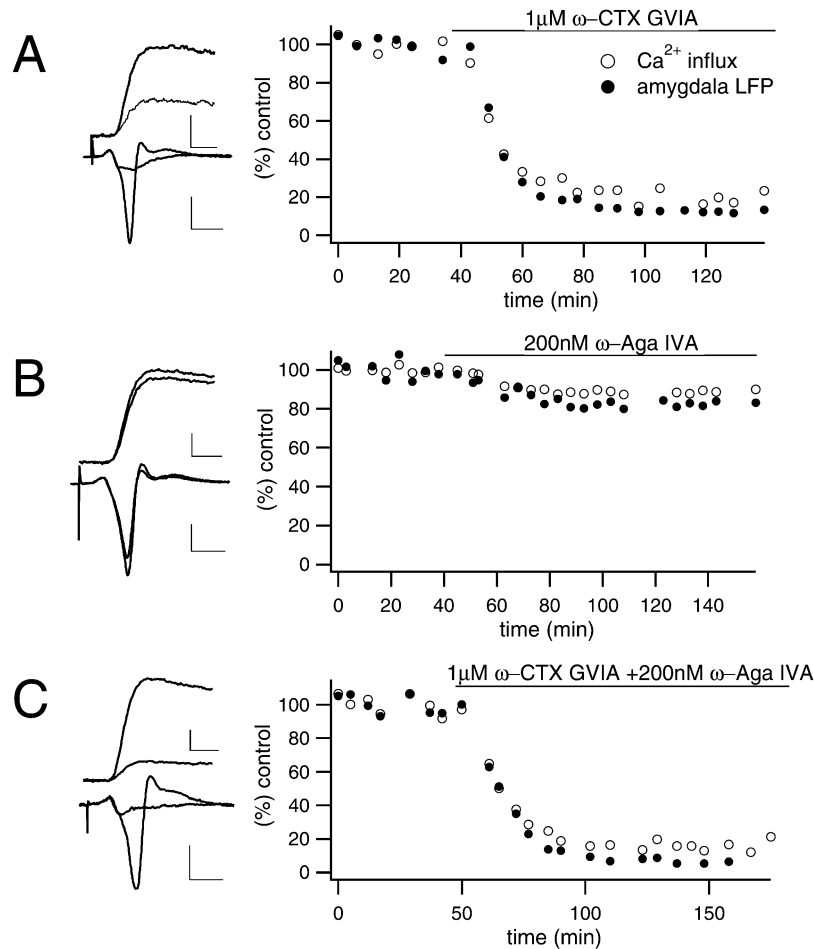


Fig. 5. Toxin effects on presynaptic Ca<sup>2+</sup> influx and amygdala LFP. Typical experiments in 1 μM ω-CTX-GVIA (A), 200 nM ω-Aga-IVA (B), and co-application of 1 μM ω-CTX-GVIA and 200 nM ω-Aga-IVA (C) showing the evoked Ca<sup>2+</sup> transients and amygdala LFP before and after application of toxins, and the time course of the block by the toxins. Transients are individual recordings, amygdala LFPs are averages of 12. For quantitative comparison between experiments, Ca<sup>2+</sup> influx and amygdala LFP measurements were derived from the average of all recordings before application of the toxins (>30 min) and all recordings after a stable baseline had been reached in the toxins. Scale bars for 20ΔF/F = 2 mV and 0.02 s.

volley remained unchanged (Fig. 5). The evoked Ca<sup>2+</sup> influx was reduced by  $92.2 \pm 2.4\%$  ( $N=5$ ) and the amygdala LFP by  $97.0 \pm 0.8\%$  ( $N=5$ ) of control (Fig. 6A, B). The reduction of Ca<sup>2+</sup> influx by co-application of the toxins was comparable to the sum of the reduction produced by each of the toxins applied separately ( $96.1 \pm 5.4\%$ ), which suggests that ω-CTX-GVIA and ω-Aga-IVA targeted separate populations of presynaptic Ca<sup>2+</sup> channels. The reduction of the amygdala LFP by co-application of the toxins is less than the sum of the reduction produced by each of the toxins applied separately ( $113.3 \pm 6.5\%$ ;  $P < 0.05$ , two-tailed  $t$ -test), suggesting that the channels are co-localized near release sites on the same presynaptic terminals,<sup>35,63</sup> and that release is driven comparably by influx through either channel type and is proportional to [Ca<sup>2+</sup>] raised to the power 1.5 or less.

Because there may be some saturation of transmission with the influx associated with 2 mM [Ca<sup>2+</sup>]<sub>o</sub>, and also because there is nearly 100% block of influx and transmission with the co-applied toxins, it is difficult to assess whether the apparent low cooperativity between

ω-Aga-IVA-dependent Ca<sup>2+</sup> influx and release is an artifact of the small effect on Ca<sup>2+</sup> influx or whether  $n$  is actually greater than 1.5, as has been observed at other synapses.<sup>35,63,66</sup> One way to approach this question is to reduce release with a combination of ω-CTX-GVIA that greatly reduces [Ca<sup>2+</sup>] influx and ω-Aga-IVA. If ω-Aga-IVA actually has a strongly non-linear effect on transmission that is masked by saturation of release when Ca<sup>2+</sup> influx is near normal, then in combination with ω-CTX-GVIA a more non-linear Ca<sup>2+</sup> influx–release relationship should emerge. We did not see any hint that the apparent cooperativity for the combined toxin application was greater than for ω-CTX-GVIA alone. That is, the apparent cooperativity was 1.4–1.5 throughout the wash-in period of the two toxins, even through the range where release was reduced sufficiently that transmission was clearly not saturated.

#### Presynaptic neuromodulation

Nothing is known about the reduction or enhancement of neurotransmitter release from frog mitral cell

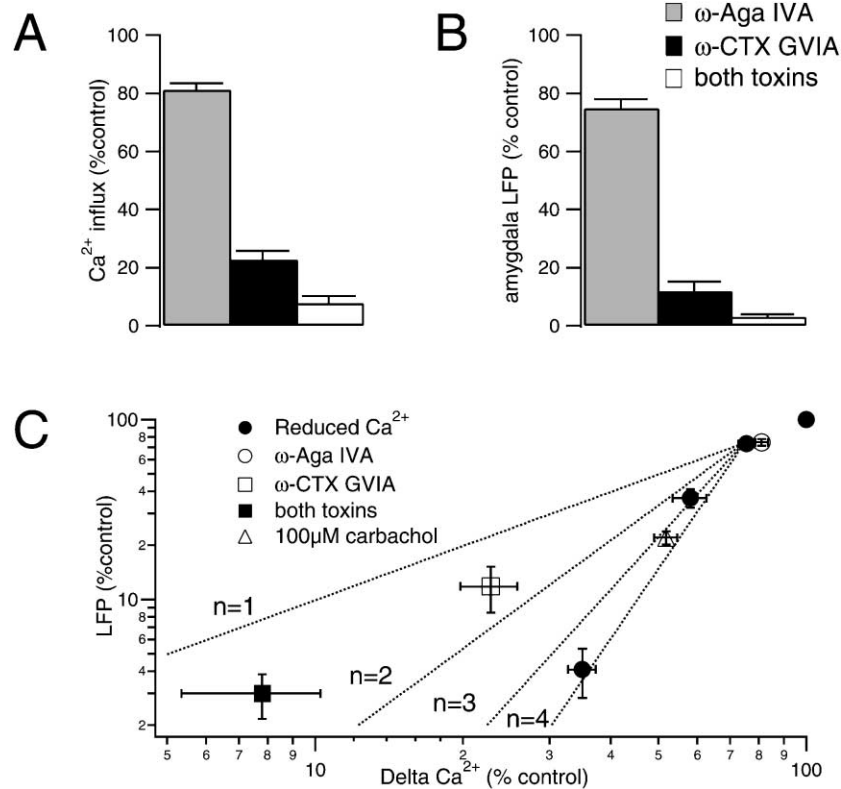


Fig. 6. Summary of the Ca<sup>2+</sup> channel toxin effects and the relationship between presynaptic Ca<sup>2+</sup> influx and amygdala LFP. (A, B) Application of 200 nM ω-Aga-IVA reduced the Ca<sup>2+</sup> influx by 18.8 ± 2.4% and the amygdala LFP by 25.2 ± 3.1% of control. The evoked Ca<sup>2+</sup> influx was reduced by 77.2 ± 3% and the amygdala LFP by 88.2 ± 3.4% of control in 1 μM ω-CTX-GVIA, and co-application of the toxins decreased the Ca<sup>2+</sup> influx by 92.2 ± 2.4% and the amygdala LFP by 97.0 ± 0.8% of control. (C) Log vs log summary of data (*N* = 5 for each toxin condition, *N* = 15 for carbachol). Ca<sup>2+</sup> influx calculated using the formula from Feller *et al.*<sup>21</sup> (see Experimental Procedures). Dotted lines correspond to  $LFP = ([Ca^{2+}]_i)^n$ , with *n* as indicated. All data are mean ± S.E.M.

terminals within the amygdala by any neuromodulatory substances. We found that the non-specific cholinergic agonist carbachol rapidly and reversibly inhibited the evoked Ca<sup>2+</sup> transient and amygdala LFP (Fig. 7A, B). On average, carbachol (100 μM) reduced the Ca<sup>2+</sup> influx to 51.8 ± 2.8% (*N* = 15) of control and the amygdala LFP to 22.1 ± 1.9% (*N* = 15) of control, without changing the threshold for AOT activation. The saturating concentration appeared to be 100 μM, since 50 μM carbachol reduced the Ca<sup>2+</sup> influx to 53 ± 6.1% (*N* = 3) of control and the amygdala LFP to 26 ± 4.9% (*N* = 3) of control, and 200 μM carbachol reduced Ca<sup>2+</sup> influx to 55 ± 4.8% (*N* = 3) of control and the amygdala LFP to 23 ± 5.6% (*N* = 3) of control (data not shown). Rinsing with ACSF returned the Ca<sup>2+</sup> influx and the amygdala LFP to control levels within 10–15 min (101 ± 1.1% and 97.8 ± 1.4%, respectively; *N* = 14).

Since we had derived relationships between suppression of Ca<sup>2+</sup> influx and transmission under conditions of Ca<sup>2+</sup> channel blockade by toxins and reduced flux per channel by lowered [Ca<sup>2+</sup>]<sub>o</sub>, we compared these to the effect of carbachol. The effect of carbachol seems to be consistent with a reduction in Ca<sup>2+</sup> influx when compared to the data from experiments where [Ca<sup>2+</sup>]<sub>o</sub> is reduced, i.e. where the flux per channel is reduced. However, carbachol's effect was significantly more non-linear, i.e.  $n = 2.54 ± 0.25$  (15 experiments), than

the block by ω-CTX-GVIA ( $t = 4.07$ ,  $P < 0.001$ ), which had a comparable effect on Ca<sup>2+</sup> influx (Fig. 6C).

To directly test whether additional postsynaptic effects on amygdala neuron excitability or input impedance were contributing to the suppression of the LFP, whole-cell recordings were made from amygdala neurons receiving monosynaptic excitatory synaptic currents from stimulation of the AOT (Fig. 7C). Biocytin filling of three recorded neurons revealed cells with sparsely branched, smooth dendrites, extending rostrally in a generally dorsolateral plane towards the telencephalon (Fig. 7). Carbachol suppressed the excitatory postsynaptic current to 25 ± 9.4% of control (*N* = 5 cells, four animals). This is the same as the suppression of the LFP in our Ca<sup>2+</sup> imaging experiments (23% of control). Two of the cells studied with voltage clamp were also recorded in current-clamp mode and showed no consistent evidence for a change in resting input impedance or membrane potential, all of which indicates a presynaptic effect of carbachol on transmitter release.

Experiments were conducted to determine whether activation of muscarinic or nicotinic acetylcholine receptors was causing the inhibition of synaptic transmission. Scopolamine (100 μM) completely blocked the inhibition of both Ca<sup>2+</sup> influx and the LFP by 100 μM carbachol in a reversible manner (Fig. 7C). Ca<sup>2+</sup> influx remained at 102.4 ± 5.5% and the amygdala LFP at

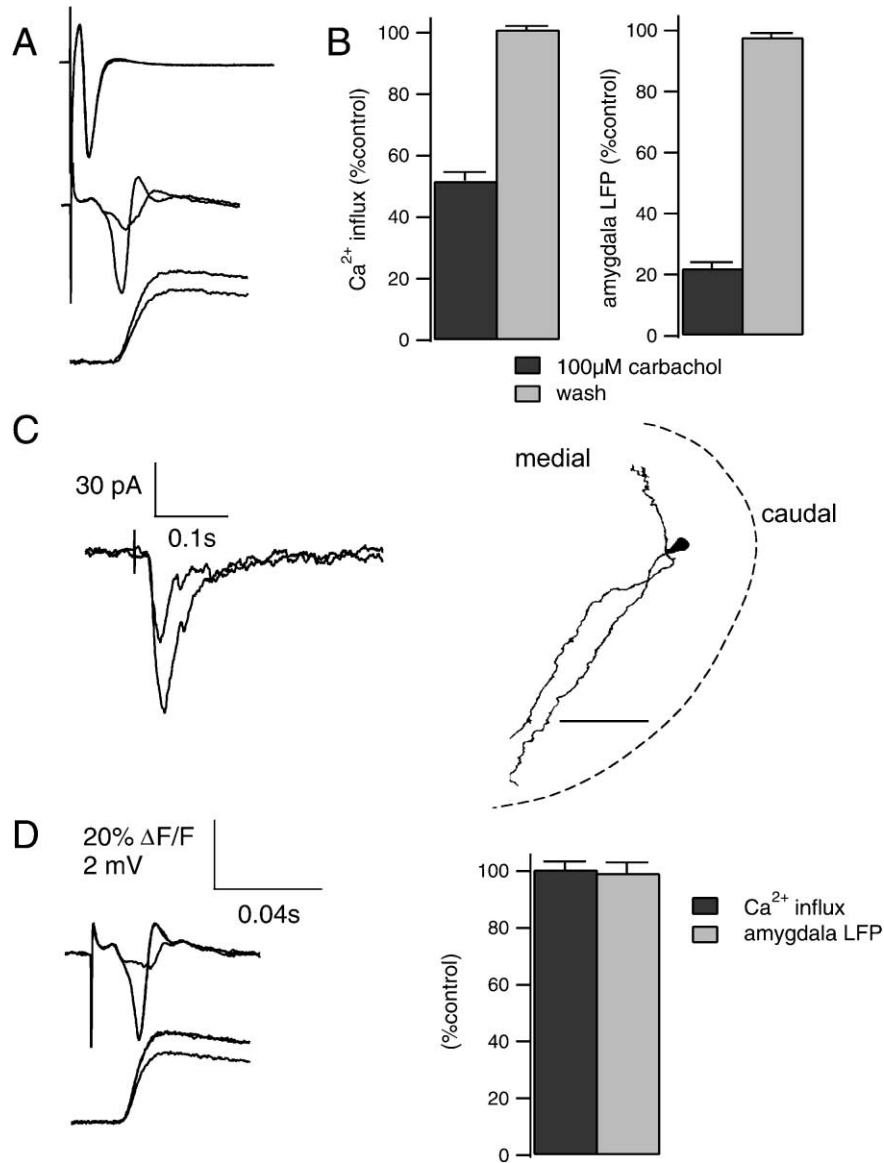


Fig. 7. Presynaptic inhibition at the mitral cell–amygdala synapse. (A) Application of 100  $\mu\text{M}$  carbachol reduces the evoked Ca<sup>2+</sup> transient and amygdala LFP, while leaving the AOT LFP unchanged (Ca<sup>2+</sup> transients are single recordings, LFPs are averages of four). The AOT LFP was recorded in the presence of 10  $\mu\text{M}$  CNQX. (B) Carbachol (100  $\mu\text{M}$ ) reduced the Ca<sup>2+</sup> influx to  $51.8 \pm 2.8\%$  ( $N=15$ ) of control conditions. Washing returned Ca<sup>2+</sup> influx to control levels ( $101 \pm 1.1\%$ ;  $N=14$ ). The amygdala LFP was reduced to  $22.1 \pm 1.9\%$  ( $N=15$ ) of control conditions. Rinsing with ASCF returned the amygdala LFP to control conditions ( $97.8 \pm 1.4\%$ ;  $N=14$ ). (C) Whole-cell excitatory synaptic currents in non-imaging experiments were suppressed by carbachol to the same extent as LFP in imaging experiments. Representative whole-cell recordings from one cell and corresponding biocytin fill of this amygdala neuron. Scale bar = 50  $\mu\text{m}$ . Dashed line shows approximate boundary of the caudal telencephalon/amygdala. Fills of two other neurons from which data on carbachol's effects were obtained showed a similar sparse, long smooth dendritic branching pattern. (D) Individual Ca<sup>2+</sup> transient and amygdala LFP recordings in control, 100  $\mu\text{M}$  carbachol, and 100  $\mu\text{M}$  carbachol plus 100  $\mu\text{M}$  scopolamine show that scopolamine blocks the carbachol-induced reduction of the Ca<sup>2+</sup> transient and amygdala LFP. Bar graph summary comparing the co-application of scopolamine and carbachol with control conditions ( $N=3$ ). All data are mean  $\pm$  S.E.M.

$99.5 \pm 1.6\%$  ( $N=3$ ) of control conditions after the co-application of carbachol and scopolamine. Nicotine (10–50  $\mu\text{M}$ ) had no effect on the Ca<sup>2+</sup> influx ( $100.6 \pm 1.2\%$  of control) or on the amygdala LFP ( $99.2 \pm 3.8\%$ ;  $N=3$ ) of control conditions (data not shown). The M1 agonist, MCN-A-343, at concentrations up to 200  $\mu\text{M}$  had no effect on the Ca<sup>2+</sup> influx ( $99.4 \pm 0.7\%$  of control) or the amygdala LFP ( $97.8 \pm 1.5\%$  of control;  $N=4$ ). 4-Diphenylacetoxy-*N*-(2-chloroethyl)-piperidine

hydrochloride (irreversible M3 antagonist; 100  $\mu\text{M}$ ) was able to block the effects of 100  $\mu\text{M}$  carbachol when co-applied (Ca<sup>2+</sup> =  $100.5 \pm 1.5\%$ , LFP =  $98.7 \pm 2.2\%$  of control;  $N=2$ ). These data suggest that the receptors are more similar to mammalian type M3 than M1 receptors.

The muscarinic block of Ca<sup>2+</sup> influx was directed towards both channel subtypes. This was tested by first applying  $\omega$ -CTX-GVIA or  $\omega$ -Aga-IVA followed by

carbachol. In one experiment, after a steady-state block of 70% of the  $\text{Ca}^{2+}$  influx was achieved with  $\omega$ -CTX-GVIA, the addition of carbachol further reduced the  $\text{Ca}^{2+}$  influx to 18% of control, corresponding to a 40% block of the remaining, mostly P/Q-type, influx. In another experiment,  $\text{Ca}^{2+}$  influx was first reduced by 15% from control levels with  $\omega$ -Aga-IVA. Addition of carbachol reduced the remaining  $\text{Ca}^{2+}$  influx to 34% of control, corresponding to a 60% block of the largely N-type  $\text{Ca}^{2+}$  influx that remained after application of  $\omega$ -Aga IVA. Further experiments will be required to determine whether there is any evidence for differential effects of presynaptic inhibition on the N versus P/Q subtypes, but these initial experiments indicate that activation of muscarinic receptors targets both  $\text{Ca}^{2+}$  channel subtypes.

## DISCUSSION

### *A model system for studying synaptic transmission*

The small size of most presynaptic terminals in the vertebrate brain prevents the use of electrodes to directly record presynaptic currents, except in the special case of the calyx of Held.<sup>22</sup> Therefore, selective loading of  $\text{Ca}^{2+}$  indicators into nerve terminals has become an important tool for the study of  $\text{Ca}^{2+}$  in synaptic transmission.<sup>21,35,43,63,66</sup> In this study, we selectively loaded mitral cell presynaptic terminals in the frog amygdala with dextran-conjugated fluorescent  $\text{Ca}^{2+}$  indicators and measured changes in free  $[\text{Ca}^{2+}]$  in terminals in the amygdala in *en bloc* preparations.

Our preparation, consisting of a telencephalic hemisphere (which can also include more rostral portions of the brain, including the brainstem), is particularly well suited for investigating physiological functioning of an intact synapse, within the context of its function in a larger circuit. All the ipsilateral fiber pathways from the accessory olfactory nerves to the diencephalon are intact and the preparation can be maintained *in vitro* for several hours at temperatures equal to those found *in vivo*, which is important considering that many processes involved in synaptic transmission are strongly temperature dependent.

Dextran-conjugated  $\text{Ca}^{2+}$  indicator dyes avoid many problems associated with acetoxymethyl loading, such as incomplete de-esterification, dye leakage or internal organelle sequestration and non-specific effects of detergents needed for solubilization. Particularly important for the present study is the fact that we can load a well-defined set of presynaptic terminals by transport along axons distant from the site of a local application of indicator. As a result, all of our fluorescence changes originate from identified presynaptic terminals from one class of projection neurons, which probably minimizes the heterogeneity of the population of terminals studied. Confocal imaging of dye-filled structures in the amygdala following injection of dye into the AOB indicated that presynaptic terminals rather than preterminal axons were the source of almost all the stimulus-evoked fluorescent transients. Although the exact process whereby dextran-conjugated dyes are taken up into neurons is

not known, several studies have confirmed the efficacy of this technique and the minimal and/or temporary damage that is associated with loading.<sup>18,20,27</sup> The separation of several millimeters between the loading site and the terminals further supports the argument that the terminals are electrophysiologically and metabolically normal.

### *Characterization of presynaptic voltage-dependent $\text{Ca}^{2+}$ channels*

We were interested in the quantitative relationship between  $\text{Ca}^{2+}$  influx and release when toxins block channels compared to when the flux per channel is reduced, as is the case with reduced  $[\text{Ca}^{2+}]_o$ . Such data may provide information about  $\text{Ca}^{2+}$  channel cooperativity in release, as well as providing information about the mechanism of action of neuromodulatory substances at presynaptic terminals.

Our estimate of the  $\Delta[\text{Ca}^{2+}]$  resulting from a single action potential is that average cytoplasmic  $[\text{Ca}^{2+}]$  is elevated approximately 60 nM, which is within the 50–150 nM range estimated for the retinotectal synapse in the frog.<sup>21</sup> At the large mossy fiber synapse in rat hippocampal slices, a single action potential produced an increase in  $[\text{Ca}^{2+}]$  of 10–50 nM,<sup>43</sup> while at the CA1 synapse an estimate of approximately 60 nM has been reported.<sup>63</sup> In the small cerebellar presynaptic terminals, estimates of the  $\Delta[\text{Ca}^{2+}]$  produced by single action potentials have been as high as 300 nM,<sup>44</sup> and for the large calyx of Held synapse in the rat brainstem 400 nM has been reported.<sup>23</sup>

Studies from various vertebrate brain regions indicate that multiple  $\text{Ca}^{2+}$  channel types support presynaptic  $\text{Ca}^{2+}$  influx and control neurotransmitter release. The proportions of the co-localized channels, as well as their relative contribution to neurotransmitter release, has been shown to vary significantly between different synapses. For example, at cerebellar parallel fiber–Purkinje cell synapses and at hippocampal CA3–CA1 synapses, there are at least three pharmacologically distinct presynaptic  $\text{Ca}^{2+}$  channels:  $\omega$ -CTX-GVIA-sensitive N type,  $\omega$ -Aga-IVA-sensitive P/Q type and a toxin-resistant R type. At hippocampal CA3–CA1 synapses, about 40% of the total  $\text{Ca}^{2+}$  transient is  $\omega$ -CTX-GVIA sensitive, 20%  $\omega$ -Aga-IVA sensitive and 40% toxin resistant.<sup>63</sup> The pharmacologically identified N- and P/Q-type channels have about equal efficacy in triggering transmitter release. At cerebellar parallel fiber–Purkinje cell synapses, 25% of the total  $\text{Ca}^{2+}$  transient is  $\omega$ -CTX-GVIA sensitive, 45%  $\omega$ -Aga-IVA sensitive and 30% toxin resistant.<sup>35</sup>

From our steady-state toxin block experiments (measurements made approximately 60 min after toxin application), we observed that, while  $\omega$ -CTX GVIA blocks 77% of the action potential-mediated  $\text{Ca}^{2+}$  influx, it was clearly less effective in blocking transmitter release compared to reducing  $\text{Ca}^{2+}$  influx by reducing  $[\text{Ca}^{2+}]_o$ . Our data indicating a nearly linear relationship between block of  $\text{Ca}^{2+}$  influx and transmitter release by  $\omega$ -CTX-GVIA are quantitatively similar to those of

Feller *et al.*<sup>21</sup> for frog retinotectal synapses, as well as those of Wu *et al.*<sup>66</sup> at single calyx synapses. These data stand in contrast to our observations that reducing Ca<sup>2+</sup> influx by reducing the flux per channel (reduced [Ca<sup>2+</sup>]<sub>o</sub>) reduces transmitter release in a strongly non-linear fashion ( $n = 3.6$ ), as observed at fast transmitting synapses throughout vertebrate and invertebrate nervous systems.

In several mammalian synapses, it appears that  $\omega$ -Aga-IVA blockade has a highly non-linear effect on the blockade of transmission.<sup>35,63,66</sup> At frog mitral cell–amygdala synapses, however,  $\omega$ -Aga-IVA blocks a small proportion of Ca<sup>2+</sup> influx, about 19%, causing a rather modest 25% reduction in transmission.<sup>21</sup> One should be a little cautious in interpreting from these data alone that  $\omega$ -Aga-IVA block of Ca<sup>2+</sup> influx is only slightly non-linearly related to block of transmission, since the Ca<sup>2+</sup> block is within the range where the extent of non-linearity could be masked by saturation of transmission. In order to properly determine whether  $\omega$ -Aga-IVA has a non-linear effect on transmission, similar to reducing [Ca<sup>2+</sup>]<sub>o</sub>,  $\omega$ -Aga-IVA should be applied under conditions where transmission will not be partially saturated. This condition was met during the wash-in of the mixture of  $\omega$ -Aga-IVA and  $\omega$ -CTX-GVIA at times when release was blocked by greater than 20%, and we noted throughout the wash-in period that the relationship between the block of Ca<sup>2+</sup> influx and transmission was described by a power relationship of approximately 1.5. If  $\omega$ -Aga-IVA-sensitive Ca<sup>2+</sup> was related to transmitter release in a strongly non-linear fashion, we would have expected a more pronounced block of transmission during wash-in of the combined toxins, which we did not see.

Since the channels blocked by the combined toxins account for >95% of Ca<sup>2+</sup> influx, we do not need to assume that there is another channel subtype that is primarily responsible for release. Furthermore, although pharmacologically defined N-type channels are responsible for a larger proportion of the Ca<sup>2+</sup> influx and transmission, both the N and P/Q subtypes appear to have a similar efficacy for supporting release, as defined by the only slightly non-linear relationship between block of Ca<sup>2+</sup> influx and transmission. Supporting the assumption that these terminals might be homogeneous in their expression of channel subtypes is the fact that they are derived from one cell type from one well-defined brain region (mitral cells from the AOB). However, even single calyx preterminals express multiple Ca<sup>2+</sup> channels that are coupled to release,<sup>66</sup> and evidence supports both segregation and co-localization of N and P/Q channels at autaptic terminals in culture.<sup>45</sup> In the absence of direct immunological data that show both subtypes are in fact co-localized to the same boutons, and that channel subtypes within a single terminal are not segregated so that each subtype is not coupled to a separate population of vesicles, we cannot exclude the possibility that the nearly linear relationship between blockade and release simply reflects complete block of Ca<sup>2+</sup> influx at a portion of the terminal (or active zones within terminals) by each toxin. However, if the relationship between influx and release were highly non-linear, then we

would expect the non-linearity to be revealed when only a portion of the channels on the terminals were blocked during wash-in of the toxin. Again, our observations during wash-in of each toxin, or the combined toxins, as cited above argue against substantial segregation of channels, since the relationship between the amount of transmission block and the Ca<sup>2+</sup> block appeared constant.

We favor the interpretation that there is minimal overlap between Ca<sup>2+</sup> microdomains for the generation of high [Ca<sup>2+</sup>] necessary for release<sup>6</sup> to explain our data that show a highly non-linear relationship between Ca<sup>2+</sup> influx and release for reduced extracellular Ca<sup>2+</sup>, but an only slightly non-linear relationship for toxin blockade. This idea is not without precedent, since direct evidence that release can be driven by Ca<sup>2+</sup> influx through a single channel has been obtained at another vertebrate synapse.<sup>53</sup> Also, Wu *et al.*<sup>66</sup> report similarly low cooperativity for  $\omega$ -CTX-GVIA block of Ca<sup>2+</sup> influx at the calyx of Held, although they favor an alternative explanation for the phenomenon at this synapse. Further studies are needed to address this issue, including comparison of the [Ca<sup>2+</sup>]<sub>o</sub>–release dose–response curve with and without toxin block, particularly for Aga-IVA toxin,<sup>45</sup> and imaging Ca<sup>2+</sup> influx into single terminals during toxin application.

#### *Presynaptic inhibition by muscarinic receptor activation*

Presynaptic modulation of glutamatergic synapses by muscarinic receptor activation is widespread in the vertebrate brain.<sup>4,5,40,41,50,54,61,62</sup> Our data indicate that presynaptic muscarinic receptor activation at mitral–amygdala synapses causes a rapid and reversible reduction in the evoked presynaptic Ca<sup>2+</sup> influx and amygdala LFP, without affecting the AOT volley. Whole-cell recordings confirm that the suppression of transmission is primarily or wholly presynaptic.

The effect of carbachol at first seems to be consistent with simply a reduction in Ca<sup>2+</sup> influx, if one compares it to experiments in which influx is reduced by lowering [Ca<sup>2+</sup>]<sub>o</sub> (Fig. 6). However, carbachol probably reduces presynaptic Ca<sup>2+</sup> influx analogous to  $\omega$ -CTX-GVIA by reducing the number of open channels rather than by changing the single channel conductance.<sup>38</sup> Therefore, it should have effects comparable to  $\omega$ -Aga-IVA and  $\omega$ -CTX-GVIA, which reduce the number of open channels, i.e. a weak effect on transmitter release relative to its block of Ca<sup>2+</sup> influx. This is not what is observed. Instead, carbachol blocks significantly more transmission than expected based on a block of Ca<sup>2+</sup> influx caused by fewer open channels. While it is also possible that a change in the kinetics of channel opening caused by carbachol could have a more non-linear effect on transmitter release relative to Ca<sup>2+</sup> influx than blockade by toxins, it has been shown at other synapses that changing the duration of action potentials, and thus the number of open channels and the average time of their opening, has a small effect on release relative to the change in Ca<sup>2+</sup> influx.<sup>15,30,70</sup> We therefore conclude that muscarinic receptor activation reduces transmission by reducing

Ca<sup>2+</sup> influx and also probably through a direct inhibitory effect on the release machinery,<sup>40</sup> while acknowledging that complex effects on channel kinetics, different from those of toxins, cannot be entirely discounted at this time.

*Acknowledgements*—Fluo-4-dextran was kindly supplied by Ian Johnson and Kyle Gee of Molecular Probes, who are also thanked for their helpful discussions of its properties. This work was supported by an NSERC Operating Grant and the Ida Steel Fund for Addiction Research to K.D.

#### REFERENCES

1. Augustine G. J., Charlton M. P. and Smith S. J. (1985) Calcium entry and transmitter release at voltage-clamped nerve terminals of squid. *J. Physiol., Lond.* **367**, 163–181.
2. Augustine G. J. and Charlton M. P. (1986) Calcium dependence of presynaptic calcium current and postsynaptic response at the squid giant synapse. *J. Physiol., Lond.* **381**, 619–640.
3. Baker P. F., Hodgkin A. L. and Ridgway E. B. (1971) Depolarization and calcium entry in squid giant axons. *J. Physiol., Lond.* **218**, 709–755.
4. Barral J., Galarraga E. and Bargas J. (1999) Muscarinic presynaptic inhibition of neostriatal glutamatergic afferents is mediated by Q-type Ca<sup>2+</sup> channels. *Brain Res. Bull.* **49**, 285–289.
5. Bellingham M. C. and Berger A. J. (1996) Presynaptic depression of excitatory synaptic inputs to rat hypoglossal motoneurons by muscarinic M2 receptors. *J. Neurophysiol.* **76**, 3758–3770.
6. Bertram R., Sherman A. and Stanley E. F. (1996) Single-domain/bound calcium hypothesis of transmitter release and facilitation. *J. Neurophysiol.* **75**, 1919–1931.
7. Borst J. G., Helmchen F. and Sakmann B. (1995) Pre- and postsynaptic whole-cell recordings in the medial nucleus of the trapezoid body of the rat. *J. Physiol., Lond.* **489**, 825–840.
8. Borst J. G. and Sakmann B. (1996) Calcium influx and transmitter release in a fast CNS synapse. *Nature* **383**, 431–434.
9. Borst J. G. and Sakmann B. (1998) Calcium current during a single action potential in a large presynaptic terminal of the rat brainstem. *J. Physiol., Lond.* **506**, 143–157.
10. Ceccarelli B. and Hurlbut W. P. (1980) Vesicle hypothesis of the release of quanta of acetylcholine. *Physiol. Rev.* **60**, 396–441.
12. Claiborne B. J., Amaral D. G. and Cowan W. M. (1986) A light and electron microscopic analysis of the mossy fibers of the rat dentate gyrus. *J. comp. Neurol.* **246**, 435–458.
13. Delaney K. R., Zucker R. S. and Tank D. W. (1989) Calcium in motor nerve terminals associated with posttetanic potentiation. *J. Neurosci.* **9**, 3558–3567.
14. Delaney K. R. and Zucker R. S. (1990) Calcium released by photolysis of DM-nitrophen stimulates transmitter release at squid giant synapse. *J. Physiol., Lond.* **426**, 473–498.
15. Delaney K. R., Tank D. W. and Zucker R. S. (1991) Serotonin-mediated enhancement of transmission at crayfish neuromuscular junction is independent of changes in calcium. *J. Neurosci.* **11**, 2631–2643.
16. Delaney K. R. and Hall B. J. (1996) An *in vitro* preparation of frog nose and brain for the study of odour-evoked oscillatory activity. *J. Neurosci. Meth.* **68**, 193–202.
17. Dodge F. A. Jr and Rahamimoff R. (1967) On the relationship between calcium concentration and the amplitude of the end-plate potential. *J. Physiol., Lond.* **189**, 90P–92P.
18. Dudkin E. A., Myers P. Z., Ramirez-Latorre J. A. and Gruber E. R. (1998) Calcium signals monitored from leopard frog optic tectum after the optic nerve has been selectively loaded with calcium sensitive dye. *Neurosci. Lett.* **258**, 124–126.
19. Eccles J. C., Sasaki K. and Strata P. (1967) Interpretation of the potential fields generated in the cerebellar cortex by a mossy fibre volley. *Exp Brain Res.* **3**, 58–80.
20. Edwards J. A. and Cline H. T. (1999) Light-induced calcium influx into retinal axons is regulated by presynaptic nicotinic acetylcholine receptor activity *in vivo*. *J. Neurophysiol.* **81**, 895–907.
21. Feller M. B., Delaney K. R. and Tank D. W. (1996) Presynaptic calcium dynamics at the frog retinotectal synapse. *J. Neurophysiol.* **76**, 381–400.
22. Forsythe I. D. (1994) Direct patch recording from identified presynaptic terminals mediating glutamatergic EPSCs in the rat CNS, *in vitro*. *J. Physiol., Lond.* **479**, 381–387.
23. Helmchen F., Borst J. G. and Sakmann B. (1997) Calcium dynamics associated with a single action potential in a CNS presynaptic terminal. *Biophys. J.* **72**, 1458–1471.
24. Katz B. and Miledi R. (1967) A study of synaptic transmission in the absence of nerve impulses. *J. Physiol., Lond.* **192**, 407–436.
25. Katz B. and Miledi R. (1967) The timing of calcium action during neuromuscular transmission. *J. Physiol., Lond.* **189**, 535–544.
26. Kemali M. and Guglielmotti V. (1987) A horseradish peroxidase study of the olfactory system of the frog, *Rana esculenta*. *J. comp. Neurol.* **263**, 400–417.
27. Kreitzer A. C., Gee K. R., Archer E. A. and Regehr W. G. (2000) Monitoring presynaptic calcium dynamics in projection fibers by *in vivo* loading of a novel calcium indicator. *Neuron* **27**, 25–32.
28. Lin J. W., Sugimori M., Llinas R. R., McGuinness T. L. and Greengard P. (1990) Effects of synapsin I and calcium/calmodulin-dependent protein kinase II on spontaneous neurotransmitter release in the squid giant synapse. *Proc. natn. Acad. Sci. USA* **87**, 8257–8261.
29. Llinas R. and Nicholson C. (1975) Calcium role in depolarization–secretion coupling: an aequorin study in squid giant synapse. *Proc. natn. Acad. Sci. USA* **72**, 187–190.
30. Llinas R., Steinberg I. Z. and Walton K. (1981) Relationship between presynaptic calcium current and postsynaptic potential in squid giant synapse. *Biophys. J.* **33**, 323–351.
31. Llinas R. R. (1982) Calcium in synaptic transmission. *Scient. Am.* **247**, 56–65.
32. Llinas R., Sugimori M. and Silver R. B. (1992) Microdomains of high calcium concentration in a presynaptic terminal. *Science* **256**, 677–679.
33. Magleby K. L. and Zengel J. E. (1982) A quantitative description of stimulation-induced changes in transmitter release at the frog neuromuscular junction. *J. gen. Physiol.* **80**, 613–638.
34. Melamed N., Helm P. J. and Rahamimoff R. (1993) Confocal microscopy reveals coordinated calcium fluctuations and oscillations in synaptic boutons. *J. Neurosci.* **13**, 632–649.
35. Mintz I. M., Sabatini B. L. and Regehr W. G. (1995) Calcium control of transmitter release at a cerebellar synapse. *Neuron* **15**, 675–688.
36. O'Donovan M. J., Ho S., Sholomenko G. and Yee W. (1993) Real-time imaging of neurons retrogradely and anterogradely labelled with calcium-sensitive dyes. *J. Neurosci. Meth.* **46**, 91–106.
37. Palay S. L. and Chan-Palay V. (1976) A guide to the synaptic analysis of the neuropil. *Cold Spring Harbor Symp. quant. Biol.* **40**, 1–16.
38. Patil P. G., de Leon M., Reed R. R., Dubel S., Snutch T. P. and Yue D. T. (1996) Elementary events underlying voltage-dependent G-protein inhibition of N-type calcium channels. *Biophys. J.* **71**, 2509–2521.

39. Peng Y. Y. and Zucker R. S. (1993) Release of LHRH is linearly related to the time integral of presynaptic Ca<sup>2+</sup> elevation above a threshold level in bullfrog sympathetic ganglia. *Neuron* **10**, 465–473.
40. Qian J. and Saggau P. (1997) Presynaptic inhibition of synaptic transmission in the rat hippocampus by activation of muscarinic receptors: involvement of presynaptic calcium influx. *Br. J. Pharmacol.* **122**, 511–519.
41. Raiteri M., Marchi M., Paudice P. and Pittaluga A. (1990) Muscarinic receptors mediating inhibition of gamma-aminobutyric acid release in rat corpus striatum and their pharmacological characterization. *J. Pharmacol. exp. Ther.* **254**, 496–501.
42. Regehr W. G. and Tank D. W. (1991) Selective fura-2 loading of presynaptic terminals and nerve cell processes by local perfusion in mammalian brain slice. *J. Neurosci. Meth.* **37**, 111–119.
43. Regehr W. G., Delaney K. R. and Tank D. W. (1994) The role of presynaptic calcium in short-term enhancement at the hippocampal mossy fiber synapse. *J. Neurosci.* **14**, 523–537.
44. Regehr W. G. and Atluri P. P. (1995) Calcium transients in cerebellar granule cell presynaptic terminals. *Biophys. J.* **68**, 2156–2170.
45. Reid C. A., Bekkers J. M. and Clements J. D. (1998) N- and P/Q-type Ca<sup>2+</sup> channels mediate transmitter release with a similar cooperativity at rat hippocampal autapses. *J. Neurosci.* **18**, 2849–2855.
46. Sabatini B. L. and Regehr W. G. (1996) Timing of neurotransmission at fast synapses in the mammalian brain. *Nature* **384**, 170–172.
47. Saggau P., Wu L. G. and Yehezkely I. (1993) Optical recording of transients of cytosolic free calcium in synaptic structures of hippocampal CA1 pyramidal cells by employing a novel selective loading technique in brain slices. *Biophys. J.* **61**, A509.
48. Scalia F. (1972) The projection of the accessory olfactory bulb in the frog. *Brain Res.* **36**, 409–411.
49. Scalia F., Gallousis G. and Roca S. (1991) Differential projections of the main and accessory olfactory bulb in the frog. *J. comp. Neurol.* **305**, 443–461.
50. Scanziani M., Gahwiler B. H. and Thompson S. M. (1995) Presynaptic inhibition of excitatory synaptic transmission by muscarinic and metabotropic glutamate receptor activation in the hippocampus: are Ca<sup>2+</sup> channels involved? *Neuropharmacology* **34**, 1549–1557.
51. Sinha S. R., Wu L. G. and Saggau P. (1997) Presynaptic calcium dynamics and transmitter release evoked by single action potentials at mammalian central synapses. *Biophys. J.* **72**, 637–651.
52. Smith S. J., Augustine G. J. and Charlton M. P. (1985) Transmission at voltage-clamped giant synapse of the squid: evidence for cooperativity of presynaptic calcium action. *Proc. natn. Acad. Sci. USA* **82**, 622–625.
53. Stanley E. F. (1993) Single calcium channels and acetylcholine release at a presynaptic nerve terminal. *Neuron* **11**, 1007–1011.
54. Sugita S., Uchimura N., Jiang Z. G. and North R. A. (1991) Distinct muscarinic receptors inhibit release of gamma-aminobutyric acid and excitatory amino acids in mammalian brain. *Proc. natn. Acad. Sci. USA* **88**, 2608–2611.
55. Takahashi T., Forsythe I. D., Tsujimoto T., Barnes-Davies M. and Onodera K. (1996) Presynaptic calcium current modulation by a metabotropic glutamate receptor. *Science* **274**, 594–597.
56. Tank D. W., Regehr W. G. and Delaney K. R. (1995) A quantitative analysis of presynaptic calcium dynamics that contribute to short-term enhancement. *J. Neurosci.* **15**, 7940–7952.
57. Tareilus E. and Breer H. (1995) Presynaptic calcium channels: pharmacology and regulation. *Neurochem. Int.* **26**, 539–558.
58. Turner T. J. (1998) Calcium channels coupled to glutamate release. *Prog. Brain Res.* **116**, 3–14.
59. Voronin L. L. (1993) On the quantal analysis of hippocampal long-term potentiation and related phenomena of synaptic plasticity. *Neuroscience* **56**, 275–304.
60. Wayson K. A., Downes H., Lynn R. K. and Gerber N. (1976) Studies on the comparative pharmacology and selective toxicity of tricaïne methanesulfonate: metabolism as a basis of the selective toxicity in poikilotherms. *J. Pharmacol. exp. Ther.* **198**, 695–708.
61. Williams S. and Johnston D. (1990) Muscarinic depression of synaptic transmission at the hippocampal mossy fiber synapse. *J. Neurophysiol.* **64**, 1089–1097.
62. Williams S. H. and Johnston D. (1993) Muscarinic cholinergic inhibition of glutamatergic transmission. In *Presynaptic Receptors in the Mammalian Brain* (eds Dunwiddie T. V. and Lovinger D. M.), pp. 57–76. Birkhauser, Boston.
63. Wu L. G. and Saggau P. (1994) Pharmacological identification of two types of presynaptic voltage-dependent calcium channels at CA3–CA1 synapses of the hippocampus. *J. Neurosci.* **14**, 5613–5622.
64. Wu L. G. and Saggau P. (1995) Block of multiple presynaptic calcium channel types by omega-conotoxin-MV1C at hippocampal CA3 to CA1 synapses. *J. Neurophysiol.* **73**, 1965–1972.
65. Wu L. G., Westenbroek R. E., Borst J. G. G., Catterall W. A. and Sakmann B. (1999) Calcium channel types with distinct presynaptic localization couple differentially to transmitter release in single calyx-type synapses. *J. Neurosci.* **19**, 726–736.
66. Zimmermann H., Volkand W., Wittich B. and Hausinger A. (1993) Synaptic vesicle life cycle and synaptic turnover. *J. Physiol., Paris* **87**, 159–170.
67. Zucker R. S. and Fogelson A. L. (1986) Relationship between transmitter release and presynaptic calcium influx when calcium enters through discrete channels. *Proc. natn. Acad. Sci. USA* **83**, 3032–3036.
68. Zucker R. S. and Lando L. (1986) Mechanism of transmitter release: voltage hypothesis and calcium hypothesis. *Science* **231**, 574–579.
69. Zucker R. S. (1993) Calcium and transmitter release. *J. Physiol., Paris* **87**, 25–36.

(Accepted 21 January 2001)